Journal of Materials Processing Technology 153–154 (2004) 596–602

Journal of Materials Processing Technology

www.elsevier.com/locate/jmatprotec

Weldability of austenitic manganese steel

J. Mendez, M. Ghoreshy, W.B.F. Mackay, T.J.N. Smith, R.W. Smith*

Department of Materials and Metallurgical Engineering, Queen's University at Kingston, Kingston, Ont., Canada K7L 3N6

Abstract

Hadfield's manganese steel, nominally Fe–1.2%C–13%Mn, is an alloy of inherent toughness, work-hardening characteristics and excellent resistance to some types of adhesive and abrasive wear. However, due to its low yield strength, it may be deformed markedly before its work-hardening become effective. In certain applications, such as railroad crossings and rock-crushers, this can be a disadvantage. In practice, when this deformation becomes excessive, welding is employed to restore the casting to its original dimensions. During welding, precautions have to be taken to avoid overheating and the attendant carbide precipitation which may lead to subsequent early failure.

Three different electrode compositions were used to overlay-weld austenitic manganese steel cast in the form of rail heads. Two of the electrodes were obtained commercially and the third was of novel chemical composition and was produced in our laboratory. Mechanical tests were then carried out to simulate the battering deformation likely to result from in-service exposure. The procedure highlighted the work-hardening characteristics and resistance to plastic flow of the weld deposit and base material, one of which consisted of the standard Hadfield's alloy whilst two others had minor transition element additions. The electrode containing molybdenum produced a weld overlay which showed better work-hardening characteristics and deformation resistance than those of the other two commercial electrodes studied.

Keywords: Austenitic manganese steel; Weldability

1. Introduction

Hadfield's manganese steel, with a composition of Fe–1.2%C–13%Mn, normally has a structure of metastable austenite which is obtained by water-quenching the steel from an annealing temperature of 1050 °C. This austenitic alloy work-hardens rapidly under repeated impact and displays remarkable toughness. This property makes the steel very useful in applications where heavy impact and abrasion are involved, such as within a jaw crusher, impact hammer, rail-road crossing (frog), etc.

Due to the low yield strength of unalloyed manganese steel, when used for rail-road components such as frogs, points and crossings, significant deformation may accrue under the enormous impact loading present during rail-road service. This causes undesirable dimensional changes to occur. In practice, rail grinding is used to maintain the geometry of the component but, eventually, overlay welding is employed to restore the original dimensions. However, the weld repair of a worn frog is expensive and incurs considerable traffic dislocation. Hence the search for a modified Hatfield alloy and an improved rebuilding procedure using appropriate welding rod compositions in order to achieve longer service life under the increasingly severe operating conditions.

Welding electrode compositions have been the subject of research since the early 1920s when one of the first electrode patents for manganese steel was issued to Churchward [1] with the compositions of 1.0–l.25% C and 3.0–13.0% Mn. Other patents have been issued since then but the general trend has been to reduce the carbon content and add some nickel to help avoid martensite formation. The smaller carbon content was intended to dilute the relatively high carbon content of the partially fused parent metal and so reduce or prevent carbide precipitation which could lead to embrittlement if the frog was not to be heat-treated after welding. However, the effects of a number of other alloying additions to the welding electrodes have been studied, e.g. Cr, Ni and even increased Mn [2]. In particular, molybdenum additions are claimed to produce weld metal that is modestly superior to that with nickel additions at the same carbon level. But this superiority would go unnoticed except in applications where the higher yield strength associated with the presence of molybdenum is utilised.

To avoid carbide precipitation during welding, it is imperative to keep the temperature of the steel below 300 °C [3]. Due to the very small thermal conductivity of Hadfield's steel, the temperature in the base metal near the welding

* Corresponding author.
E-mail address: smithrw@post.queensu.ca (R.W. Smith).

0924-0136/$ – see front matter © 2004 Elsevier B.V. All rights reserved.
doi:10.1016/j.jmatprotec.2004.04.033

zone could exceed 300 °C during welding. Therefore all welding procedures should be such as to maintain local temperatures below 300 °C. This makes arc welding the only recommended process for welding and hard facing manganese steel, because of the relatively short period of heating involved. According to Avery et al. [4], to prevent embrittlement of the base metal, the temperature of the zone 12 mm from the weld should not exceed 250 °C.

The present work was undertaken to determine the changes in the microstructure of the weld and heat-affected zone of various Hadfield's steel for which the composition had been modified slightly. Molybdenum- and nickel–chromium-bearing electrodes were used to verify the superiority of the former in the mechanical properties of the weld deposit as claimed by Avery et al. [4]. A third electrode bearing chromium and similar to the one used by Canadian Pacific Electrode [5] for building up worn frogs and crossings, was used also.

In order to quantitatively test the various electrodes and base metal combinations, two sets of apparatus were constructed. A rail/wheel impact simulator [6] was designed and constructed to apply a repeated impact to the specimens. A second piece of equipment was constructed in order to produce massive deformation in the test specimen of base metal and weld deposit by dropping a known weight on the sample from a fixed height.

The effects of these two methods of testing on the work-hardening characteristics and the resistance to plastic flow of the alloys were investigated.

2. Experimental procedure

The raw material used in alloy preparation was low carbon rail-stock to which were made alloy additions to obtain the desired nominal compositions, as shown in Table 1. The charge was melted in an induction furnace and cast into a dried sand old from a pouring temperature of 1450 °C. The old pattern consisted of a rail head of 4.2 in height, 12.5 cm in length and 6 cm in width. Due to the low thermal conductivity of austenitic manganese steel [7], it was unnecessary to cast any of the web section of a standard rail. Thus, only the head of the rail was cast as rail component for this welding study.

Table 1
Nominal and actual alloy compositions for railhead casting (wt.%)

Classification	C	Mn	Mo	V
Standard Hadfield (R3)	1.2	12	–	–
Standard Hadfield (R3)[a]	1.19	12.15	–	–
Low carbon–1%V (R9)	0.8	12	–	1
Low carbon–2%V (R7)	0.8	12	–	2
Low carbon–2%V (R7)[b]	0.82	12.8	–	1.93
Low carbon–1%Mo (R10)	0.8	12	1	–

[a] Modified Hadfield's steels.
[b] Actual analysis results. Total other elements is less 0.5% and the remainder is Iron.

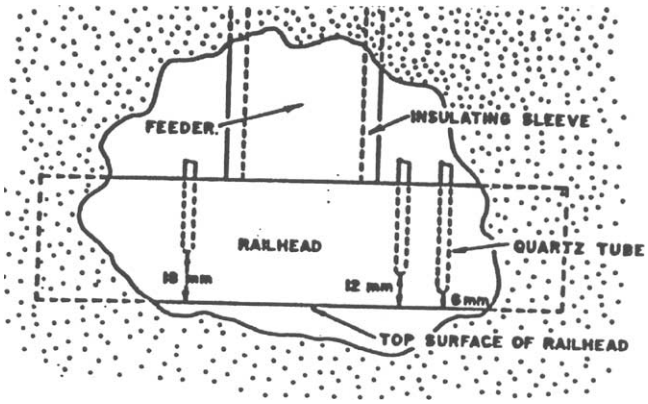

Fig. 1. Cutaway view of railhead sand mould.

Olivine sand was selected as a old material due to its low reactivity properties for austenitic manganese castings [8]. To obtain sound castings, it was necessary to use an insulating riser sleeve.

Three quartz tubes 4 mm I.D. were arranged in the sand in such a way that their closed end were located at 6, 12 and 18 mm, respectively, from the surface of the rail to be welded, as shown in Fig. 1. These tubes provided the holes for thermocouples to be inserted to record the temperature at the given location during welding at the surface of the rail. Before welding, the as-cast rail heads were first austenitised at 1150 °C for 2 h [9] in a controlled argon atmosphere to avoid decarburisation [10,11] and then quenched in water.

The use of a submerged arc as the welding process made it necessary to use electrodes of the wire type. Table 2 shows the electrodes that were available commercially in 3 mm diameter size. The other was the molybdenum electrode which had been produced in quartz tube of 4 mm I.D. This has been done by forcing liquid metal into the quartz tube by means of vacuum. The cast rods were welded autogenously (no filler metal) to each other by gas-tungsten welding to provide sufficient electrode length for a 17.5 cm weld pass along the full length of the rail head. An automatic submerged arc welding machine was used in the experiment. To obtain suitable welding conditions, the following criteria were established:

(a) the temperature of the zone beyond 12 mm from the weld surface should not exceed 300 °C, and
(b) the weld pool should be approximately 2 cm wide.

Table 2
Nominal composition of the welding electrodes

Classification	C	Mn	Cr	Ni	Mo	Si	Fe
Chromium[a]	0.23	16.54	16.61	0.91	0.05	0.56	65.1
Nickel–chromium	1.0	13.7	4.7	3.7	–	0.4	76.5
Molybdenum	0.8	13	–	–	1	–	85.2

[a] Canadian Pacific Electrode [4].

Table 3
Welding parameters for the two electrodes

Diameter (mm)	Volt	Ampere	Burn-off rate (cm/min)	Traverse speed (cm/min)	Deposition rate (g/min)
2.78	43	105	109.2	11.4	40
4	43	105	44.5	9.1	38.9

Using the 2.78 and 4 mm diameter electrodes, a number of weld beads were laid on the rail heads at different burn-off rates and traverse speeds. Also for every welding pass made the temperature in the rail head at 6, 12 and 18 mm from the welded surface were recorded using a three channel chart recorder. The welding parameters used are shown in Table 3.

The sequence of sample preparations for post-welding studies is shown in Fig. 2. Deformation studies were carried out in two ways. The rail/wheel impact simulator, Fig. 3, was used in an attempt to simulate in the specimen the deformation of a frog under service conditions. The specimen was placed in the sample holder and then mounted in the fly-wheel of the machine, Fig. 3b.

The fly-wheel was rotated at 30 rpm. Spacers were used under the specimen to change the height of the sample after a given number of impacts. The maximum specimen height above the surface of the sample holder was 2 mm for base metal and 3 mm for weldment, and the static applied load was 22,370 N.

During the test, the specimen was periodically removed from the equipment and the overall length measured. The difference in length was taken as a measure of the amount of plastic flow occurring under the conditions and duration of testing.

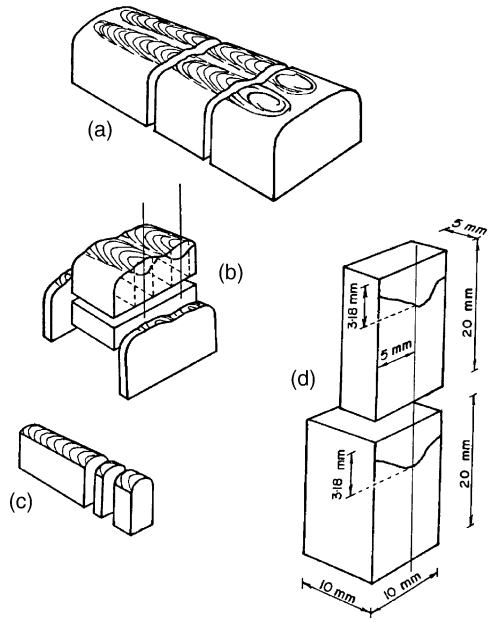

Fig. 2. Specimen preparation for work-hardening and plastic deformation.

The other testing equipment used was the Weight Drop Machine. This device was used to study the effect of massive and rapid deformation on the weldment. For this test, a 72 kg load was dropped from a height of 2.5 m onto a specimen which had been glued on an anvil.

3. Results and discussion

3.1. Thermal analysis

Due to the very low thermal conductivity of austenitic manganese steel (7.6% of the thermal conductivity of a low carbon steel) [7], it was important to evaluate the maximum depth of the rail head which was unaffected by the "informal" heat-treatment of overlay welding height from the surface. The results from the temperature measurement are shown in Fig. 4.

Fig. 4 shows the maximum temperature reached in the thermocouples located at various defects from the upper surface of the rail. Although the temperature recorded by the last thermocouple was lower than the values of the steady state region, this did not influence the outcome of the temperature survey. The plateau in the temperature suggests that a steady state condition was reached and maintained for approximately 7 cm of rail.

3.2. Compression test

Fig. 5 shows the results obtained from the compression tests on the samples from the base metal using the railway simulator. The values shown in the figure are the average of four specimens with a typical standard deviation of 0.14–0.28. Both the alloys R7 and R9 proved to be the most resistant materials to plastic flow of those tested. The standard Hadfield's steel (R3) appeared to have a deformation of approximately 25% over the strongest material tested, R7. Specimen R10 showed the least resistance to deformation of all the steels tested. At the end of the test (240 impacts with railway simulator), the surface hardness of the deformed sample was recorded and the average value for each specimen calculated, Table 4. Specimen R3 appeared to have the best work-hardening characteristic, followed by R10. This might be due to little resistance of these alloys to plastic flow in comparison with R7 and R9. Microstructural examination of deformed samples of R3 and R10 showed no significant differences between the two alloys. This indicates that the addition of 1% molybdenum to the low carbon Hadfield's

Table 4
Average hardness of Hadfield's manganese alloys

	R3	R7	R9	R10
Hardness (Rc)[a]	49	45	45	47
Standard deviation	1.41	1.11	0.75	1.11

[a] Average of seven hardness determinations.

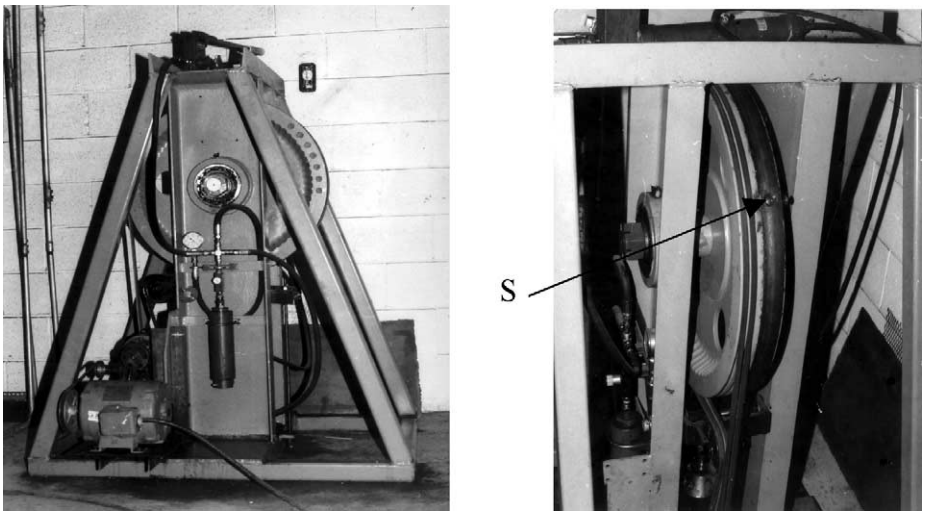

Fig. 3. Rail/wheel impact simulator: (a) general view; (b) specimen location on flywheel marked 'S'.

steel (R10) does not alter the formation of twins appreciably, Fig. 6. The microstructural information is in accordance with the similarity in the plastic deformation characteristics exhibited by these alloys, Fig. 6. The microstructure of R7 and R9 in which V was added to the low carbon Hadfield's steel shows a sharp decrease in the number of twins; although both alloys display many, the dendritic structure and its associated carbide segregation, together with the formations of twins seems to account for high resistance of these alloys to plastic deformation, Fig. 7.

The result of compression testing on the weldment specimens (weld deposit and base metal combined) as they were subjected to an increasing number of impacts is shown in Fig. 8. The hardness value shown in this figure are the average of seven hardness determinations with a typical standard deviation of 0.39–2.67. In the "as-welded" condition, the molybdenum deposit was slightly harder than the nickel–chromium and chromium weld-rod deposits. The same trend was observed throughout the duration of the test. However, the hardness of the weld metal deposited by the molybdenum electrode rose rapidly and continued to work-harden slowly with increasing number of impacts. In contrast, there was no significant differences in the work-hardening characteristic of the nickel chromium and chromium deposits, although the former showed slightly lower hardness values consistently. The maximum hardness of both weld deposits was unaffected by continued testing.

The evaluation of the plastic deformation characteristics of the weld deposit as well as that of the weldment was carried out on 5 mm × 10 mm × 20 mm specimens, Fig. 2, using a maximum height of 2.5 mm above the sample holder and, as noted earlier, a maximum static applied load of 22,370 N.

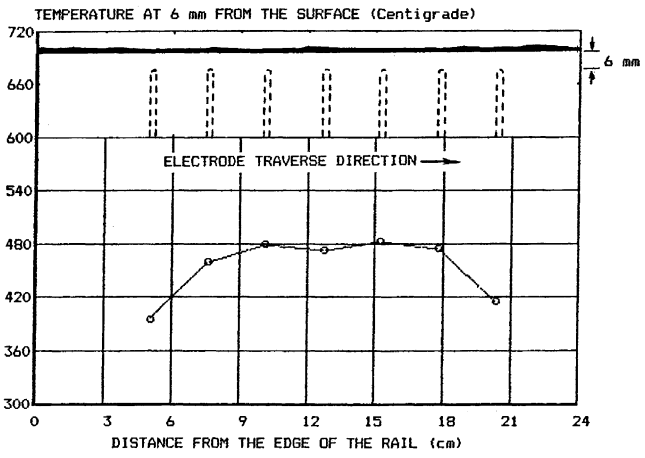

Fig. 4. Welding temperatures in a railhead.

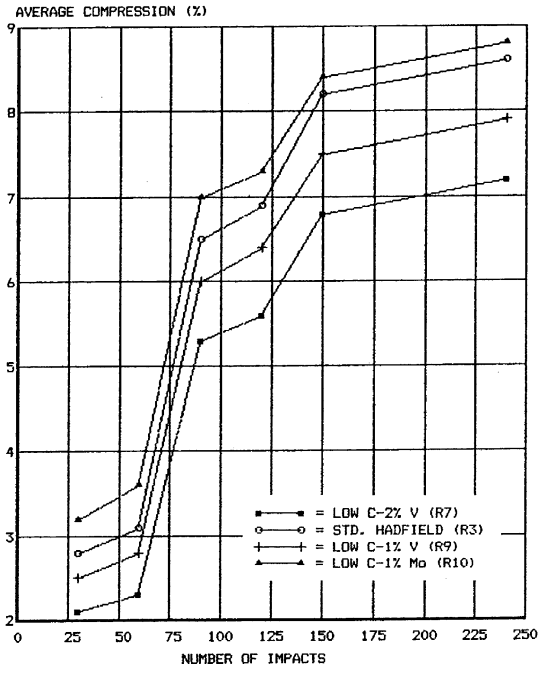

Fig. 5. Impact compression of Hadfield's manganese alloys.

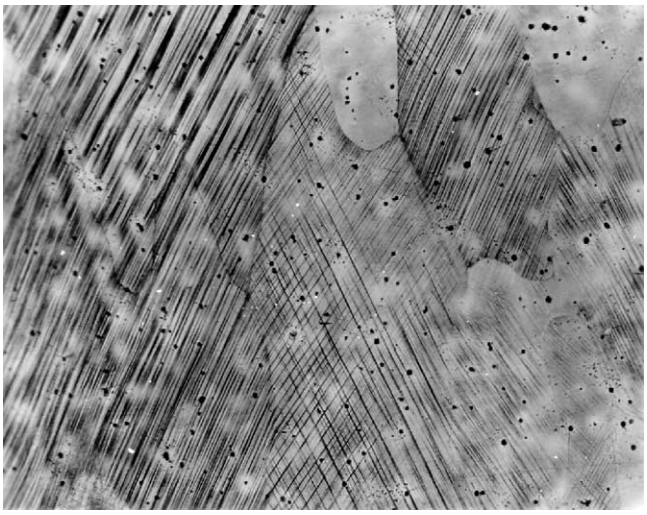

Fig. 6. Deformed low carbon–1%Mo modified Hadfield's manganese steel (R10) (50×).

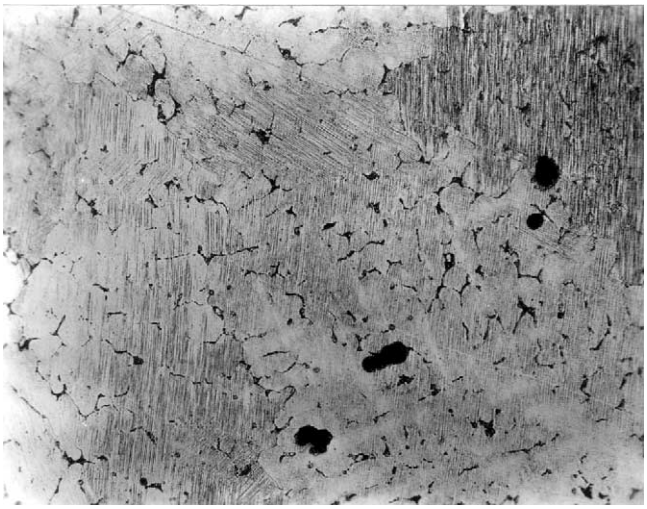

Fig. 7. Deformed low carbon–2%V modified Hadfield's manganese steel (R7) (50×).

The results of testing all the weld deposit steel combinations are summarised in Table 5. The compression values reported in this table are the average of four specimens with a typical standard deviation of 0.16–0.32. After the test period (360 impacts), the plastic deformation characteristics

Table 5
Average compression values of the weldment and weld deposit (%)

	Hadfield's manganese alloys							
	R3		R7		R9		R10	
	WM	WD	WM	WD	WM	WD	WM	WD
Molybdenum	9.3	18.6	8.5	25.3	8.7	23.0	10.2	16.8
Nickel–chromium	9.6	20.0	8.9	28.0	9.3	26.2	11.0	20.1
Chromium	10.6	25.1	8.8	30.3	9.4	27.1	10.5	19.9

WM: weldment and WD: weld deposit.

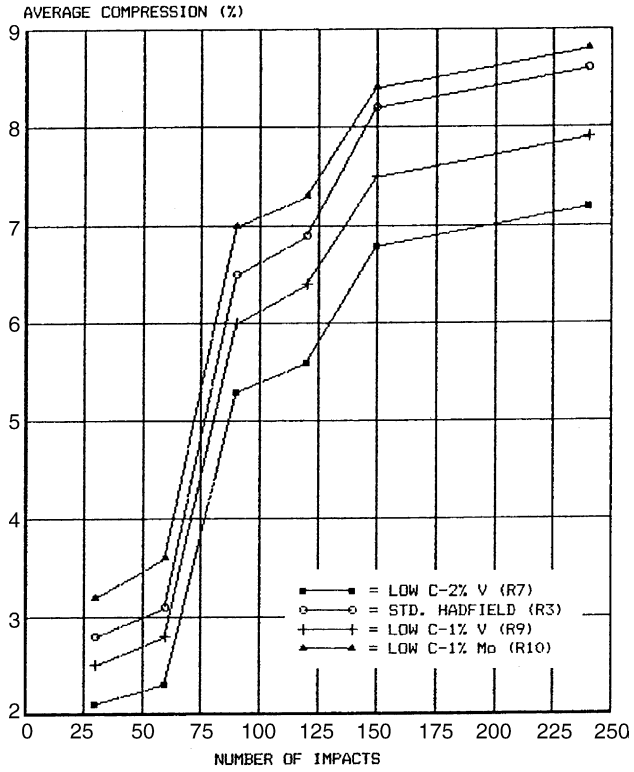

Fig. 8. Work-hardening characteristics of weld deposits.

of the molybdenum deposit on the four different steels appeared consistently better than the other steel companies. These showed a minimum deformation of 16.8% on R10 and a maximum of 25.3% on R7 as compared to 20–28 and 19–30% deformation for the Ni–Cu and Cr deposits, respectively.

Fig. 9a–c consists of photomicrographs of deformed weldment specimens showing the weld interface of the different electrode composition on alloy R7. All the weld deposits exhibited a cellular-dendritic structure and approximately the same amount of deformation twinning. The nickel–chromium and chromium deposit show relatively larger inclusions located mainly along the grain boundaries. Also the latter shows larger grains. These two effects together may be the reason for the low plastic flow resistance of the chromium weld deposit. On the other hand, the molybdenum weld deposit, Fig. 10, shows smaller inclusions which appear to be more uniformly dispersed in the matrix than along the grain boundary. This and the deformation twins may account for its excellent work-hardening characteristic and resistance to plastic deformation.

Comparison tests were also carried out on the weight drop device to study the effects of massive and rapid deformation on the work-hardening characteristics of the weld deposits. At the end of the test, the surface hardness values of the deformed weld deposit were recorded for each electrode composition. These showed a drop in average hardness of each weld deposit as compared with the average hardness values obtained by the rail/wheel impact simulator. A decrease of up

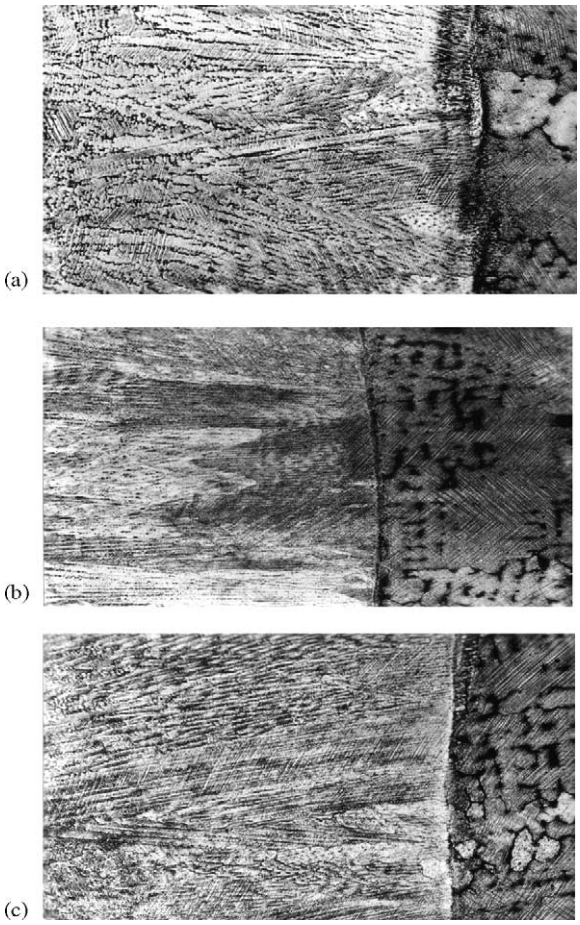

Fig. 9. (a) Deformed weld interface of nickel–chromium weld deposit on R7 (50×); (b) deformed weld interface of chromium weld deposit on R7 (50×); (c) deformed weld interface of molybdenum weld deposit on R7 (50×).

to 20% in hardness was observed in the molybdenum weld deposit. Similarly, a drop in hardness of 10% was observed in both the chromium and the nickel–chromium deposits.

A microstructural analysis of the samples deformed with the weight drop device shows significant twinning but not as much as expected since the amount of deformation twinning developed in the microstructure using this test would be more or less the same as that observed by using the rail/wheel impact simulator. Thus, it appears that rapid, massive deformation does not allow the structure to fully develop its work-hardening potential.

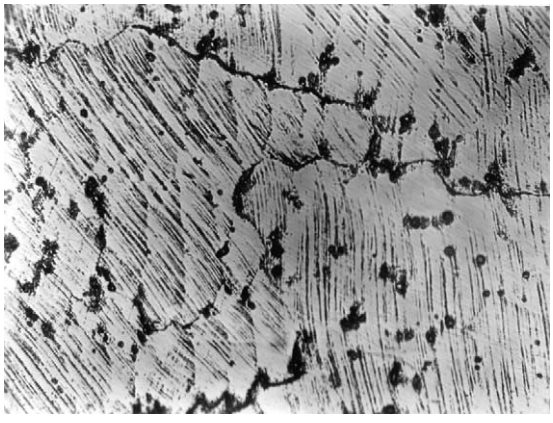

Fig. 10. Deformed molybdenum weld deposit (500×).

This is particularly significant as Kotechi and Rajan [2], in a study of the influence increased Mn and Mn–Cr contents on the work-hardening capacity of the weld deposit, report that a drop-weight test was found to offer better discrimination than standard tensile or hardness testing. It should be noted that these are effectively single load applications, whereas the industrial situations in which austenitic manganese steels are used typically involve repeated applications of load, e.g. a rail wheel on a frog, a hammer crushing rock.

The subject of this paper has been the rebuilding of austenitic manganese rail track components, although other applications can be considered. However, it is difficult to find economic data for such rebuilding, and the extent to which the installation of a frog with improved properties might be cost-effective.

Dahl et al. [12] report that, in Sweden, the cost of the weld repair of a frog is approximately 20% compared to the installation of a new frog. They also report on their optimum method of laying down the weld overlay.

Often the frog is bolted to the adjoining rails for convenience and to avoid the carbide embrittlement of the frog if it is welded in place. However, Bartoli and Digioia [13] suggest how such welding attachments may be achieved without embrittling the frog.

A question still to be answered by the rail carrier industry is what work-hardening capacity and impact strength is adequate for a heavy haul railway frog; since axle loads appear to gradually creep-up, ‘as high as possible’ seems to be the answer!

Of particular interest to the foundryman is the extent to which the purchaser of (say) frogs is likely to pay an appropriate premium for superior frogs. In Canada, most certainly, CP rail would like to be able to install a frog with a 50% increase in the service life from the present figure of 140 million gross t. The most expensive alloying additions used in our Hadfield’s Steel Development Programme to date would increase the charge cost/frog by 200–300%. However, many of the elements are now relatively abundant, e.g. tungsten, and so the price would fall dramatically with increased consumption. A detailed cost benefit analysis of using a 200 million gross t frog, compared with the present version would be interesting. It is clear that the initial casting price is a small part of the total cost of a frog, i.e. purchased casting, straightening, grinding off the decarburised layer, explosive hardening, fitting, installation, rebuilding (usually twice), and finally replacement.

4. Conclusions

1. It was shown that the plastic deformation and work-hardening characteristics of the molybdenum weld

deposit were significantly better than those of the weld metal deposited using commercial nickel–chromium and chromium electrodes.

2. There was no significant difference between the nickel–chromium and chromium weld deposits with respect to work-hardening and plastic flow upon deformation.
3. The low carbon–1%V and –2%V Hadfield steel exhibited excellent resistance to deformation, but low work-hardening characteristics.
4. The work-hardening characteristics of the weld deposits were appreciably reduced when subjected to massive deformation.
5. It was found when using the molybdenum bearing electrode that the extent of deformation of the base metal in order of increasing deformation was (1) low carbon–1%Mo, (2) standard Hadfield's steel, (3) low carbon–1%V and (4) low carbon–2%V. However, the overall measured deformation of the weldments was less in this case than when using the nickel–chromium and the chromium electrodes.

References

[1] J. Churchward, US Patent No. 1,377,543 (1920).
[2] D.J. Kotechi, V.B. Rajan, Weld. Res. Suppl. (July 1998) 293–298.
[3] Roll Crusher Maintenance, Rebuilding, and Repair, Pit and Quarry, October 1970, pp. 104–106.
[4] H.S. Avery, et al., Weld. J. 33 (5) (1954) 459–479.
[5] E. Taylor, Private Communication, Canadian Pacific Railway, 1981.
[6] T. Smith, B.Sc. Thesis, Department of Mechanical Engineering, Queen's University, Kingston, Ont., Canada, February 1982.
[7] N. Tsujimoto, AFS I.C.M.J. 4 (2) (1979) 62–77.
[8] C.W. Farrar, J. Iron, Steel Inst. 202 (1964) 543.
[9] W.B.F. Mackay, R.W. Smith, CIGGT Report No. 82-6, Queen's University, Kingston, Ont., Canada, October 1982.
[10] S.B. Sant, R.W. Smith, J. Mater. Sci. 22 (1987) 1808–1814.
[11] C.H. White, R.W.K. Honeycombe, J. Iron Steel Inst. 200 (1979) 457.
[12] B. Dahl, B. Mogard, B. Gretoft, B. Ulander, In situ railtrack repair and reclamation by welding, Weld. Rev. Int. (February 1996) 19–22.
[13] M. Bartoli, M. Digioia, Manganese steel castings: new technology for welding frogs to rail, Transport. Res. Rec. 1071 (1986) 39–43.